Physics of Fluids ARTICLE pubs.aip.org/aip/pof

Spatiotemporal distribution of the intraglottal pressure and vocal fold contact pressure in excised larynges

Cite as: Phys. Fluids **37**, 097114 (2025); doi: 10.1063/5.0283313
Submitted: 30 May 2025 · Accepted: 13 August 2025 ·
Published Online: 3 September 2025

Sarah Lehoux and Zhaoyan Zhang[a)]

AFFILIATIONS

Department of Head and Neck Surgery, University of California, Los Angeles, California 90095-1794, USA

Note: This paper is part of the Special Topic, Flow and Phonation.
[a)]**Author to whom correspondence should be addressed:** zyzhang@ucla.edu

ABSTRACT

The contact pressure experienced by the vocal folds during phonation is considered a major factor contributing to vocal fold injuries and lesions. Understanding the spatiotemporal distribution of vocal fold contact pressure across the medial surface and its dependence on laryngeal geometrical and mechanical properties (such as glottal gap, vocal fold vertical thickness, vocal fold length, and vocal fold stiffness) is essential to identifying strategies that minimize contact pressure and reduce the risk of vocal injury. This study aims to characterize the spatiotemporal distribution of intraglottal pressure across the medial surface in excised larynges. The intraglottal pressure was measured using a modified probe microphone at different locations within the vertical plane containing the glottal centerline (mid-sagittal plane), following a grid-like pattern. The resulting pressure distribution maps indicate small variations of intraglottal pressure in the anterior–posterior dimension, but large, complex variations in the vertical dimension. A criterion, derived from applying Bernoulli's equation to vocal fold vibration with prescribed vocal fold contact, was developed to identify the contact pressure peak as a rapid increase in the intraglottal pressure preceded by a negative pressure in the intraglottal pressure waveform. This criterion also allows estimation of the vertical span of vocal fold contact (by extension the vocal fold vertical thickness) and the mucosal wave speed. The preliminary results from this study indicate that the vocal fold vertical thickness has a large impact on the peak contact pressure value, which corroborates findings from previous computational studies.

I. INTRODUCTION

The human voice originates in the larynx, where the two vocal folds vibrate and collide with each other repeatedly. Overuse or misuse of the voice can lead to vocal fold tissue trauma (phonotrauma) and benign lesions such as polyps or nodules, which often negatively impact voice quality and quality of life. The contact pressure (also known as impact stress) experienced by the vocal folds during collision is considered a major factor in contributing to phonotrauma[1,2]. Clinical voice care, such as resonant voice therapy[3,4], often aims at increasing vocal efficiency to minimize contact pressure and reduce the risk of phonotrauma *in vivo*. However, the distribution of contact pressure across the medial surface of the vocal folds is rather complex. Many important aspects of vocal fold contact pressure, such as the location of maximum contact pressure, the variations of contact pressure distribution when modifying laryngeal geometrical and mechanical properties, or the accurate identification of the contact pressure peak in the intraglottal pressure waveform, are not well understood. Therefore, there is a need to better understand the spatiotemporal distribution of the vocal fold contact pressure and its dependence on laryngeal physiology, to identify strategies that minimize contact pressure and reduce the risk of phonotrauma *in vivo*, and to improve clinical voice care.

Previous studies have proposed various methods of measuring intraglottal pressure and contact pressure in excised larynges[2,5,6], physical vocal fold models[7–9], and in living human subjects[10,11]. Those studies generally utilized a pressure sensor placed between the vocal folds to measure intraglottal pressure, from which contact pressure was then identified. Generally, those studies showed important effects of laryngeal configuration in geometry and stiffness and subglottal pressure on the magnitude of contact pressure. Most notably, Jiang and Titze[2] observed that contact pressure increases with increasing subglottal pressure and decreases with increasing glottal gap. Increasing vocal fold length also has the effect of increasing contact pressure up to a certain point, beyond which contact pressure starts

decreasing with further increase in vocal fold length. Additionally, numerical simulations by Zhang[12–14] showed that other parameters, such as the vertical thickness of the vocal folds and the narrowing of the epilarynx, could have notable effects on the contact pressure value that, however, were never confirmed experimentally.

Due to the difficulty in accessing the vocal fold medial surface, previous studies often measured contact pressure at a few locations over the medial surface rather than a detailed mapping of the contact pressure distribution over the medial surface. Throughout a vocal fold oscillation cycle, the glottal airway changes its shape alternately from vertically convergent to divergent (or less convergent), due to a surface wave (often referred to as mucosal wave) propagating vertically along the vocal fold medial surface. Because of this continually varying medial surface shape, the location of vocal fold contact is not fixed but moves continuously within one oscillation cycle[15], which may significantly impact the contact pressure distribution over the medial surface along both the vertical and anterior–posterior directions. Additionally, any change in laryngeal adjustments, such as the glottal gap, vocal fold vertical thickness, or vocal fold stiffness, can have a large effect on the spatiotemporal distribution of vocal fold contact pressure.

Previous studies often reported an intraglottal pressure waveform containing a sharp peak, corresponding to the contact pressure generated from vocal fold collision[2,7,11], followed by a more rounded, longer peak, corresponding to the aerodynamic intraglottal pressure generated by a convergent glottal shape during glottal opening[16–18]. This observation is often used to identify the instant of vocal fold contact in the intraglottal pressure waveform and determine the magnitude of peak vocal fold contact pressure. However, identification of the contact pressure peak in the intraglottal pressure waveform is not always straightforward, particularly when the intraglottal pressure waveform deviates from this typical waveform shape. For example, Alipour and Scherer[6] reported intraglottal pressure waveforms that generally do not possess a secondary peak, making the identification of contact pressure less obvious, even though they used a very similar setup to the one used in the study by Jiang and Titze[2]. Identification of the contact pressure peak can also be more difficult when the intraglottal pressure waveform exhibits strong ripples due to acoustic resonances from either the subglottal or supraglottal tract, as shown in our data below. Thus, a physics-based approach in identifying the instant of vocal fold contact in the intraglottal pressure waveform is desirable.

To address these issues, this study proposes to quantify the spatiotemporal distribution of intraglottal pressure and contact pressure in the vertical plane containing the glottal centerline (mid-sagittal plane) along both the vertical and anterior–posterior dimensions. Intraglottal pressure was measured by a sensor with a small sensing area (less than 0.2 mm^2), allowing a high spatial resolution measurement of the intraglottal pressure distribution. While physical models typically allow better control on vocal fold geometry and mechanical parameters as well as high reproducibility, excised larynges were used in our study such that the intraglottal pressure distribution can be investigated in a realistic vocal fold vibration pattern exhibiting a clear mucosal wave, with continuous variations in the location and instant of vocal fold contact during one oscillation cycle. Experiments were performed using a full-larynx setup, where both vocal folds are present, as well as a hemilarynx setup, where one vocal fold is surgically removed to allow a medial view of the vibrating vocal fold. The geometrical and mechanical properties of the vocal folds were modified within each larynx through sutures simulating the action of laryngeal muscles. From the intraglottal pressure waveform, the instant of contact and the peak contact pressure were determined based on theoretical prediction and visual experimental confirmation. The goals of the study are to obtain a fine resolution "map" of the intraglottal pressure to better understand the forces applied to the vocal fold medial surface, to provide a physics-based methodology to more accurately identify contact pressure, and to observe changes in the contact pressure distribution across different laryngeal configurations in geometry, stiffness, and position.

II. METHODS

A. Full-larynx experimental setup

In the full-larynx experiments, three human larynges were obtained from a 40 year-old man, a 79 year-old man, and a 77 year-old woman. The larynges were obtained from autopsy and stored in a freezer at −80 °C. The night before the experiment, the larynges slowly thawed in a fridge at −4 °C, and on the day of the experiment, they were taken out of the fridge and thawed to room temperature while regularly sprayed with phosphate buffered saline solution. Supralaryngeal tissues were removed to expose the vocal folds, and sutures were attached bilaterally to the larynges for the control of vocal fold adduction and elongation, mimicking the actions of the lateral cricoarytenoid and cricothyroid muscles, respectively. Various weights were attached to the sutures to change the degree of adduction or elongation in a symmetrical manner (the same degree of adduction and elongation was applied to the left and right vocal fold).

The larynges were mounted on a tracheal tube with a uniform cross-sectional area of 1.84 cm^2, and screws were used to secure the cricoid cartilage in place [see Figs. 1(c)–1(e) (Multimedia view)]. The tracheal tube was connected to an expansion chamber, resulting in a distance of approximately 13 cm between the expansion chamber and the level of glottal entrance. Airflow was delivered to the larynges through a pressurized air source, after being warmed and humidified with a Hudson RCI ConchaTherm III device (Teleflex, Morrisville, NC, USA). Airflow rate was measured by a mass flow meter (model 0258B-00050SV, MKS Instruments, Inc., Andover, MA, USA) upstream from the subglottal expansion chamber. Two adaptors were mounted on the tracheal tube for the measurement of the mean and acoustic components of the subglottal pressure. A probe microphone type 4182 (Brüel and Kjaer, Naerum, Denmark) with a 50 mm-long probe measured the acoustic component of the subglottal pressure, while a vacuum pressure transducer (model 220DD-00100A2B, MKS Instruments, Inc., Andover, MA, USA) measured the mean subglottal pressure. Both sensors were mounted flush with the tracheal wall, approximately 7 cm below (upstream from) the glottal entrance. A half-inch pressure-field microphone type 4193 (Brüel and Kjaer, Naerum, Denmark) was used to measure the outside sound at a 25 cm distance from the vocal folds. This microphone has a relatively flat frequency response between 0.07 Hz and 20 kHz. No vocal tract was used in this study.

Intraglottal pressure was measured using a modified 100 mm-long probe tube with a diameter of 1.24 mm, attached to another probe microphone type 4182. The modification of the probe tube consisted of closing the open end of the probe tube with solder and making a small hole on the side of the probe, about 20 mm from the now-closed end [see Figs. 1(a) and 1(b)], similarly to the study by Chen and Mongeau[7]. The side hole was the sensing element where intraglottal

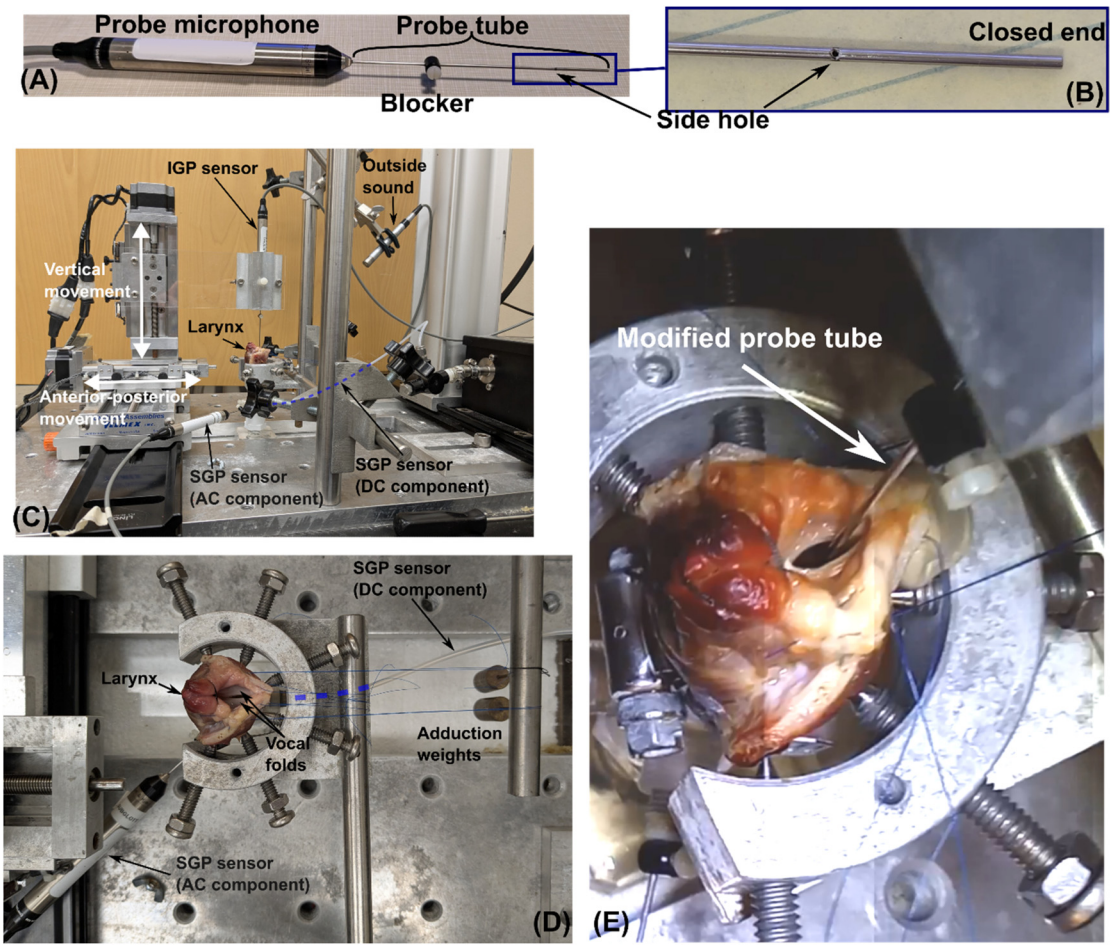

FIG. 1. Description of the full larynx experimental setup; SGP: subglottal pressure, IGP: intraglottal pressure. (a) Probe microphone with the modified probe attached. The blocker is fixed to the probe only to indicate the direction of the side hole (the sensing element). (b) Zoom in on the tip of the probe, showing the sensing element in more detail. (c) Overview of the full larynx setup showing all pressure sensors and the step motor system. (d) Larynx attachment to stabilize the cricoid cartilage, and the sutures used for vocal fold adduction and elongation. (e) Close-up view of the larynx with the modified probe tube placed between the vocal folds. Multimedia available online.

pressure was measured, and its diameter was approximately 0.45 mm, resulting in a sensing area of approximately 0.16 mm^2. A blocker [see Fig. 1(a)] was secured around the probe tube to indicate the direction the sensing element was facing. The intraglottal pressure microphone was then attached to a mechanical arm connected to two step motors [see Fig. 1(c)] that allowed vertical (inferior–superior) and anterior–posterior movement of the intraglottal pressure probe within the vertical plane that contains the glottal centerline (i.e., the mid-sagittal plane). This placement of the probe at the glottal centerline allows measurement of the air flow pressure when the vocal fold is not in contact with the probe and the contact pressure between the vocal folds and the probe when the vocal fold facing the sensing element comes in contact with the probe. This contact pressure is only an approximation of the contact pressure between the two vocal fold medial surfaces, which is impossible to measure directly without a probe obstructing the motion of the vocal folds.

The two motors were independently controlled through a Matlab script, and all signals (mean airflow rate, mean subglottal pressure, intraglottal pressure, outside sound, subglottal acoustic pressure) were simultaneously recorded and digitized at a sampling rate of 50 kHz using two data acquisition cards NI-9215 (National Instruments, Austin, TS, USA) connected in a NI cDAQ-0178 chassis (National Instruments, Austin, TS, USA). Data collection was made at different locations within the mid-sagittal plane, each 250 ms long, following a grid pattern with 51 points spanning 10 mm along the vertical dimension and 5 points spanning 4 mm along the anterior–posterior dimension, resulting in a 0.2 mm resolution in the vertical dimension and a 1 mm resolution in the anterior–posterior dimension. At the beginning of each experiment, the initial position of the probe tube was set: the microphone was placed so that the probe tube was between the two vocal folds, with the sensing element facing the right or left vocal fold, the vertical position was adjusted so that the sensing element was slightly above the vocal folds during phonation (i.e., in the supraglottal space), and the anterior–posterior location was adjusted so that the probe was slightly posterior from the middle of the membranous glottis. Care was taken to place the probe tube at the glottal centerline so

that it had a similar impact on both vocal fold vibrations. However, accurate identification of the centerline was difficult because of inherent laryngeal asymmetry and the finite size of the tube. The probe can be seen inside the glottis while the vocal folds are oscillating in Fig. 1(e) (Multimedia view).

For brevity, only the data obtained with the larynx from the 40 year-old man are reported here. However, the overall pattern of the contact pressure distribution over the medial surface was similar in the other larynges.

B. Hemilarynx experimental setup

For the hemilarynx experiments, three larynges were harvested from mongrel dogs that were sacrificed for a different research project and stored in a −80 °C freezer. The same protocol was applied to those larynges for thawing and preparation. In addition, the right vocal fold was surgically removed to expose the medial surface of the left vocal fold.

The larynges were mounted on the same tracheal tube, and an acrylic plate was used to replace the excised vocal fold [Fig. 2(d)]. The acrylic plate had a T-shaped slot where a separate acrylic piece can slide vertically [Figs. 2(a)–2(c)]. This acrylic sliding piece was machined as two halves glued together [Fig. 2(a)] and contained a S-shaped channel inside [see Figs. 2(a) and 2(c)]. The inferior end of the channel was used as the pressure sensing element where intraglottal pressure was measured [Figs. 2(a), 2(b), and 2(d)], while an insert was glued to the superior end of the channel [Fig. 2(b)] where a 50 mm-long probe tube (attached to a probe microphone type 4182) was connected. The S-shaped channel was designed to allow pressure waves to propagate from the sensing element to the microphone membrane without hindering the visibility of the vocal fold from a medial point of view. The sensing element had an ellipsoidal shape with an area of about 0.19 mm^2. The larynges were pushed against the acrylic plate with prongs and sealant paste was used to seal the gaps [as demonstrated in Fig. 2(d)]. The sliding acrylic piece and the probe microphone were attached to a custom 3D-printed part fixed to the mechanical arm connected to the two step motors. Due to the difficulty of moving the acrylic plate in the anterior–posterior dimension without modifying the laryngeal configuration, intraglottal pressure was recorded only at one location along the anterior–posterior dimension in the hemilarynx experiments.

Two high-speed cameras were used to simultaneously capture the motion of the vocal fold from a medial view (Phantom v711, Vision Research, Wayne, NJ) and from a superior view (Phantom v210, Vision Research, Wayne, New Jersey) at 10,000 frames per second. An additional NI-9263 card (National Instruments, Austin, TS, USA) was used to output a trigger signal so that both cameras were triggered synchronously with the pressure measurement. The medial surface was also tattooed with Indian ink and a prism was used to obtain a stereoscopic view of the medial surface for three-dimensional reconstruction of the medial surface, which will be reported in a future study.

Similarly to the full-larynx experiments, only the data from one larynx are reported here for brevity.

C. Data processing

For each laryngeal configuration, the airflow rate was adjusted so that phonation was strong and stable. The acoustic subglottal pressure

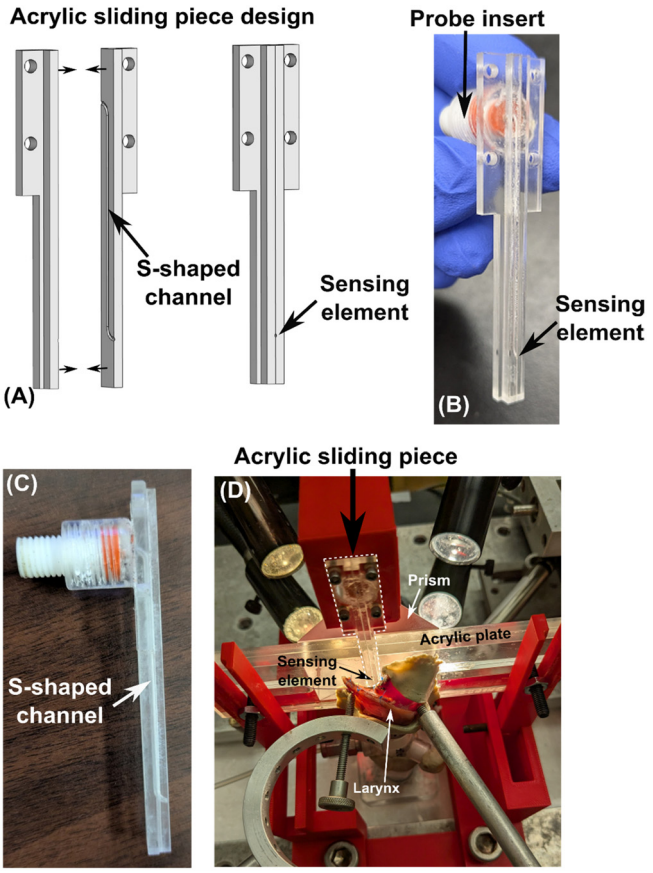

FIG. 2. Description of the acrylic sliding piece used in the hemilarynx setup. (a) 3D representation of the piece design as two halves that were glued together. The left view shows the two separate halves, making the inside S-shaped channel visible, while the right view shows the piece with the two halves glued together. The lower end of the S-shaped channel is the sensing element. (b) Photograph of the acrylic sliding piece, showing the probe tube insert glued to the acrylic piece. (c) Photograph of the acrylic sliding piece where the S-shaped channel is visible inside. (d) Overview of the hemilarynx setup, where the acrylic sliding piece is contoured by dashed white lines.

waveform was used to synchronize data collected at different locations over one oscillation cycle. More specifically, the highest peak of the subglottal pressure waveform within one cycle was used as a reference instant to synchronize all other signals collected at different locations. This way, the intraglottal pressure distribution along the vertical and anterior–posterior dimensions can be monitored and compared within one vocal fold oscillation cycle.

D. Calibration of the probe microphones

The probe microphones type 4182 have a relatively flat frequency response between 1 Hz to 20 kHz, and the use of probe tubes create a smooth high-frequency roll-off. However, the addition of the side hole during the full-larynx experiments and the use of the acrylic sliding piece during the hemilarynx experiments had an unknown effect on the frequency response of the probe microphone. To compensate for this effect, the frequency responses of the intraglottal pressure sensor

(the probe microphone attached to the modified probe for the full-larynx setup, and the probe microphone with a 50 mm-long probe tube connected to the acrylic piece for the hemilarynx setup) and of the acoustic subglottal pressure sensor (probe microphone attached to an unmodified 50 mm-long probe tube) were simultaneously measured using a loudspeaker playing a logarithmic chirp. The transfer function between those two systems was then calculated as the ratio between the Fourier transform (averaged over 10 repetitions) of the signal measured by the intraglottal pressure sensor and the Fourier transform (averaged over 10 repetitions) of the signal measured by the acoustic subglottal pressure sensor. After each experiment, the pressure signals recorded by the intraglottal sensor were calibrated by first calculating their Fourier transform, then multiplying it by the transfer function, and finally performing an inverse Fourier transform. Both probe microphones were individually calibrated by the manufacturer and a unique calibration factor indicating the sensitivity (output voltage for a given pressure, in mV/Pa) was provided for each microphone. All microphones were connected to a NEXUS conditioning preamplifier (Brüel and Kjaer, Naerum, Denmark) that allowed to increase or decrease the individual gain of each microphone by steps of 10 dB. Adjusting the pressure signals with this gain allowed to obtain the value of the oscillating pressure in Pa.

III. RESULTS

A. Intraglottal pressure distribution and variations along the vertical (inferior–superior) and anterior–posterior dimensions

Figure 3 presents the dynamic distribution of the intraglottal pressure along both the vertical and anterior–posterior dimensions, for a set of recordings made during the full-larynx experiments. Here, a weight of 50 g was attached to each of the adduction sutures, and no weight was attached to the elongation sutures. In addition, the thyroid cartilage was pushed posteriorly to shorten the vocal folds, increase their thickness, and make them lax. The mean subglottal pressure was about 2.3 kPa and the fundamental frequency was about 128 Hz. Each of the panels (a)–(e) shows the variations of the intraglottal pressure within one oscillation cycle (horizontal axis) and along the superior–inferior dimensions (vertical axis). The corresponding acoustic subglottal pressure waveform is also shown above each panel. Different panels show the spatiotemporal pressure distribution at different anterior–posterior locations. Here, the pressure "maps" (and all the subsequent ones) show the normalized intraglottal pressure, which corresponds to the value of the intraglottal pressure divided by the mean subglottal pressure.

From Fig. 3, it appears that the variations of the intraglottal pressure along the anterior–posterior dimension are rather small, especially compared to the variations in the vertical dimension. The slight variations along the anterior–posterior dimension could be attributed to the slight variations in the vocal fold vibration pattern over the duration of the experiment: the time needed to measure the intraglottal pressure at all chosen locations across the medial surface was about 4 minutes for the full-larynx experiments, during which the vocal folds were continuously oscillating, potentially incurring slight variations in their vibration pattern. The slight variations in the acoustic subglottal pressure waveform in each panel of Fig. 3 also suggest small changes in the vibration patterns. There are no visible substantial variations in the maximum value of the intraglottal pressure across different anterior–posterior positions.

One interesting result from this figure is the large variations of the intraglottal pressure along the vertical dimension. The intraglottal pressure is low and shows only small variations in the superior part of the panels, which corresponds to the supraglottal region right above the

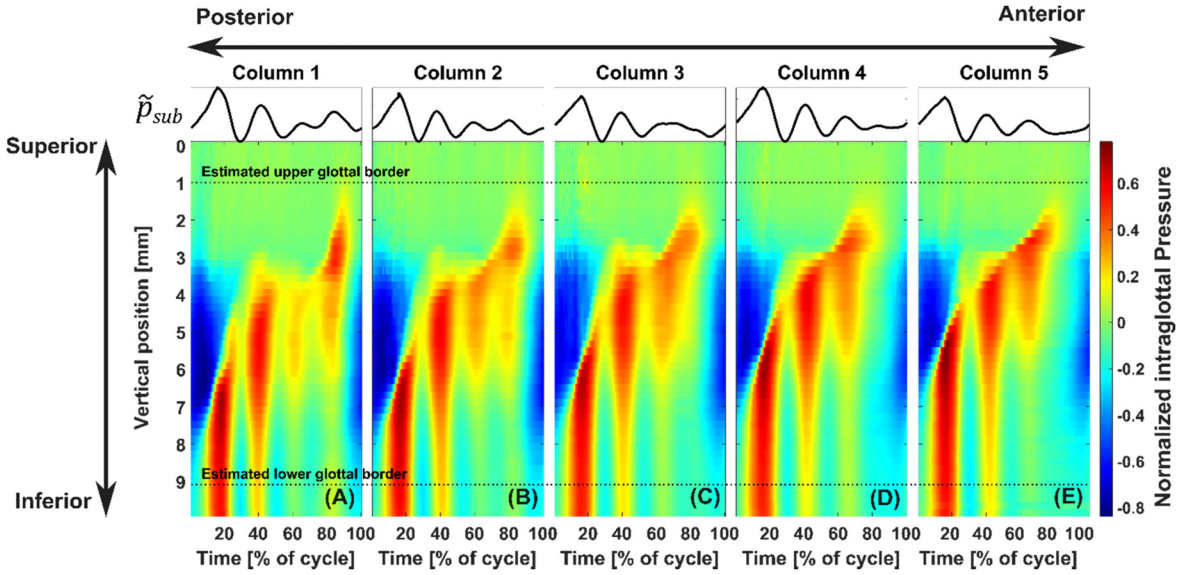

FIG. 3. Spatiotemporal distribution of normalized intraglottal pressure. Here, a weight of 50 g was attached to each adduction suture, and no weight was attached to the elongation sutures. In addition, the thyroid cartilage was slightly pushed posteriorly to make the vocal folds thick and lax. The mean subglottal pressure was about 2.3 kPa and the fundamental frequency was about 128 Hz. Each of the panels (a)–(e) corresponds to a different position along the anterior–posterior dimension. Within each panel, the normalized intraglottal pressure is presented as a map showing its value along time (horizontal axis) and superior–inferior dimension (vertical axis). The corresponding acoustic subglottal pressure waveform is also presented above each panel. Rough estimates of the upper and lower glottal borders are indicated by dotted black lines.

vocal folds. On the opposite end, in the lower part of the figure, the intraglottal pressure waveform is very similar to the subglottal pressure waveform, which suggests the probe was in the subglottal space. Although it is not possible to accurately locate the upper and lower glottal borders, Fig. 3 indicates rough estimates of those borders as black dotted lines.

Between those two ends of the laryngeal space, the intraglottal pressure waveform varies greatly with the vertical position. This is clearly visible also on Fig. 4, which depicts the intraglottal pressure waveform at different vertical positions. In Fig. 4(b), the variations are shown for the upper (superior) part of the spatiotemporal map, corresponding to the transition region between the supraglottal and intraglottal spaces. As the probe goes downwards from the supraglottal space, a peak appears in the intraglottal pressure waveform around 8 ms. Since this peak occurs just before the highest subglottal acoustic pressure peak (around 10 ms), which often corresponds to glottal closure at the lower margin of the medial surface[19,20], it is unlikely the peak around 8 ms is associated with vocal fold contact.

Further below, more peaks start appearing [see Figs. 4(c) and 4(d)] in the intraglottal pressure waveform. Some of those peaks occur in the same instants as the peaks of the ripples in the subglottal pressure waveform, indicating that they are most likely related to the peaks of the subglottal pressure due to subglottal acoustic resonances. Other peaks are not related to a specific acoustic resonance event. The highest peak in the intraglottal pressure waveform occurs at row 35 at an instant right after the instant of peak acoustic subglottal pressure, indicating that this is likely the instant of first vocal fold contact. However, further confirmation is required.

B. Identification of the contact pressure peak

Full-larynx experiments do not allow visual confirmation of the time-varying contact area on the medial surface, and therefore are not sufficient to identify, with certainty, the contact pressure component in the intraglottal pressure waveform. In addition, the presence of strong ripples in both intraglottal and acoustic subglottal pressure waveforms adds another layer of difficulty for confidently identifying the contact pressure peak, as similar ripples are not present in the intraglottal pressure waveforms shown in the previous studies.[2,5–7,9,11]

In this case, it is possible to use knowledge from the expected behavior of intraglottal pressure during vocal fold oscillation. This behavior can be expressed through Bernoulli's equation (the derivation of this equation and associated assumptions are detailed in Appendix)

$$p = P_{sup} + (P_{sub} - P_{sup})\left(1 - \frac{{A_{sep}}^2}{A^2}\right), \quad (1)$$

where p is the intraglottal pressure at the location of interest, P_{sup} is the supraglottal pressure (assumed to be equal to 0 in our case because the excised larynges were not attached to a vocal tract), P_{sub} is the subglottal pressure (set to 1 kPa in our case), A_{sep} is the time-varying glottal area at the location of flow separation [set to be at the level of the upper vocal fold margin for simplicity[17]—see Fig. 5(a)], and A is the time-varying glottal area at the location of interest. A typical pressure map predicted using this equation when applied to vocal fold vibration with a prescribed vocal fold contact pattern is displayed in Fig. 5. In Fig. 5(b), the mean component of the intraglottal pressure was removed to keep only

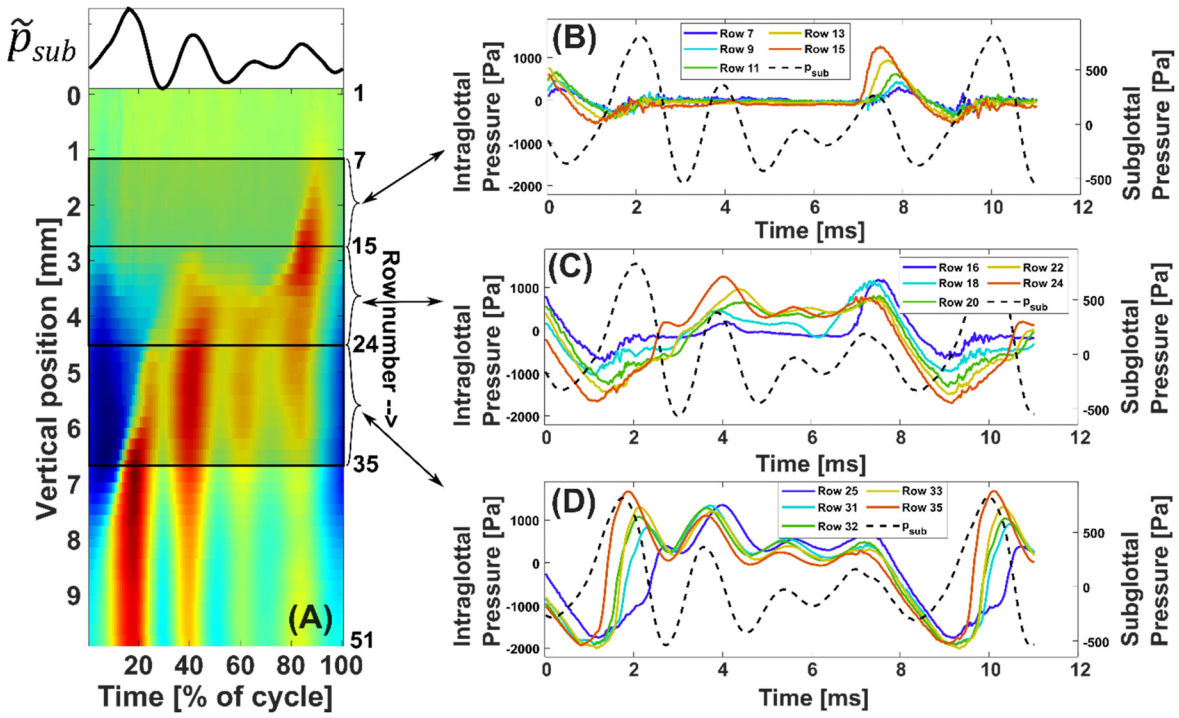

FIG. 4. Changes in the intraglottal pressure waveform along the vertical dimension. The left panel (a) shows the spatiotemporal map of the intraglottal pressure. Panels (b)–(d) show the corresponding time-varying intraglottal pressure waveforms at various locations along the vertical dimension, as well as the acoustic subglottal pressure (p_{sub}) waveform in dashed black lines. The row number corresponds to the vertical position of the probe. The row number increases toward the inferior direction.

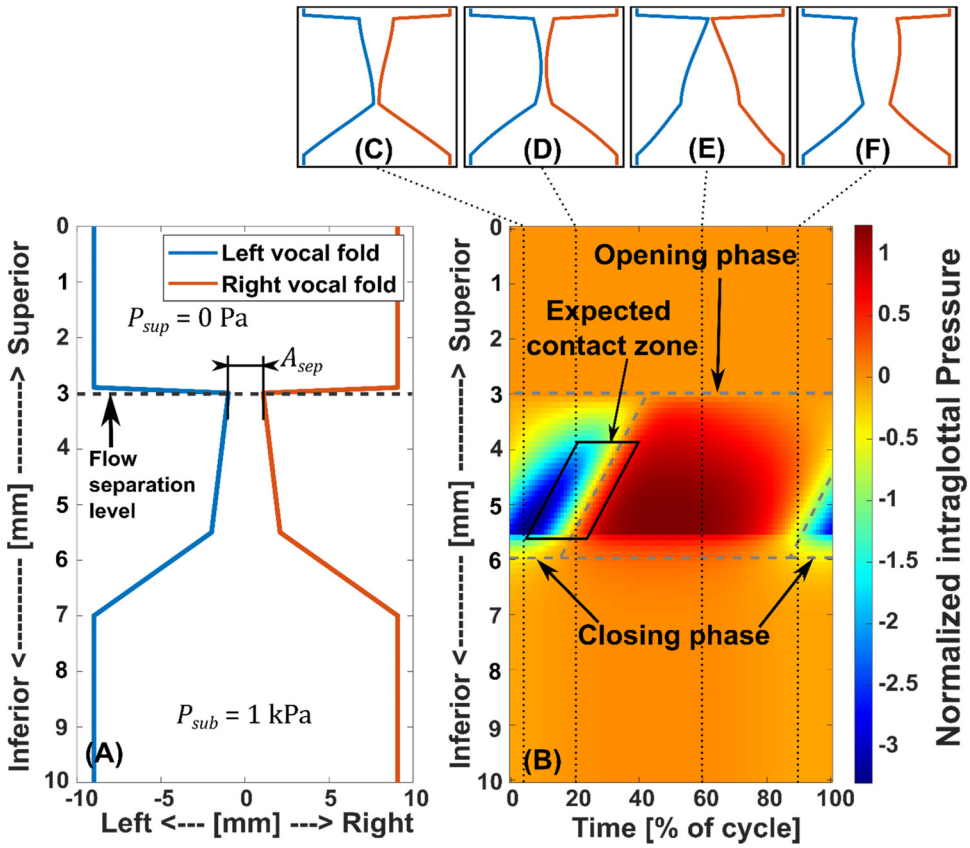

FIG. 5. Results from numerical simulations using Bernoulli's equation and a simple vocal fold geometry, shown on panel (a). Panel (b) displays the pressure distribution calculated with Bernoulli's equation and prescribed vocal fold vibration. For convenience, the opening and closing phases are indicated with dashed gray lines, and a parallelogram with plain black contour indicates the zone where vocal fold contact is expected to occur. The shape of the medial surface is shown on top of panel (b) for four different instants: during the closing phase (c), transitioning from closing to opening phase (d), during the opening phase (e), and transitioning from opening to closing phase (f).

the acoustic component and to allow comparison with our experimental results. Additionally, the parameters of the model (geometry and amplitude of vibration) were adjusted so that the minimum glottal area was small but never equal to zero, to avoid singularity.

This model, although simple, provides important insights about the expected intraglottal pressure pattern during one oscillation cycle: during glottal closing, the glottal airway shape is generally divergent [see Fig. 5(c)]; therefore, the glottal area A at the lower margin of the medial surface is smaller than the glottal area at the flow separation level A_{sep} and the intraglottal pressure is negative. Because the contact pressure component of the intraglottal pressure waveform is expected to occur at and after the instant of glottal closure, this means that the contact pressure peak should occur right after this negative intraglottal pressure. The zone where vocal fold contact is expected to occur is indicated with a parallelogram (plain black contour) in Fig. 5(b). In other words, vocal fold contact is preceded by a negative intraglottal pressure and followed by a rapid increase in intraglottal pressure. In Fig. 4(d), this corresponds to the intraglottal pressure peaks occurring around 2 and 10 ms (red line). These two peaks also coincide with the largest subglottal pressure peak, indicating the instant of glottal closure[19]. Using the same criterion, it can be determined that the peak at 8 ms in Fig. 4(b) is not associated with vocal fold contact. In the intraglottal region, as the mucosal wave propagates upward, vocal fold contact is lost permanently at around 4.5 mm in the vertical dimension, corresponding to about row 24 in Fig. 4(c). Similarly, the transition from the intraglottal to the subglottal space can be observed in the pressure maps through the changes in the waveshape of the intraglottal pressure: as the probe goes downward (inferiorly), the contact pressure peak in the waveforms below row 35 (not shown in Fig. 4) becomes less sharp as its rising slope decreases, and the preceding negative pressure becomes less negative. Vocal fold contact is lost at about 8 mm in the vertical dimension, indicating this is the location of the initial vocal fold contact. Thus, in this case (Fig. 4), the vertical span of vocal fold contact is about 3.5 mm.

To further confirm the identification of the contact pressure peak, we used the high-speed video images of the medial surface recorded during the excised hemilarynx experiments to visually correlate the instant of vocal fold contact against the sensing element with the corresponding peak in the intraglottal pressure waveform. Figure 6 (Multimedia view) shows an example of the intraglottal and subglottal pressure waveform [Fig. 6(g) (Multimedia view)] together with the captured high-speed video images [Figs. 6(a)–6(f) (Multimedia views)] at six instants of interest. In this figure, part of the acrylic channel is seen on the video frames [Figs. 6(a)–6(f) (Multimedia views)] and the

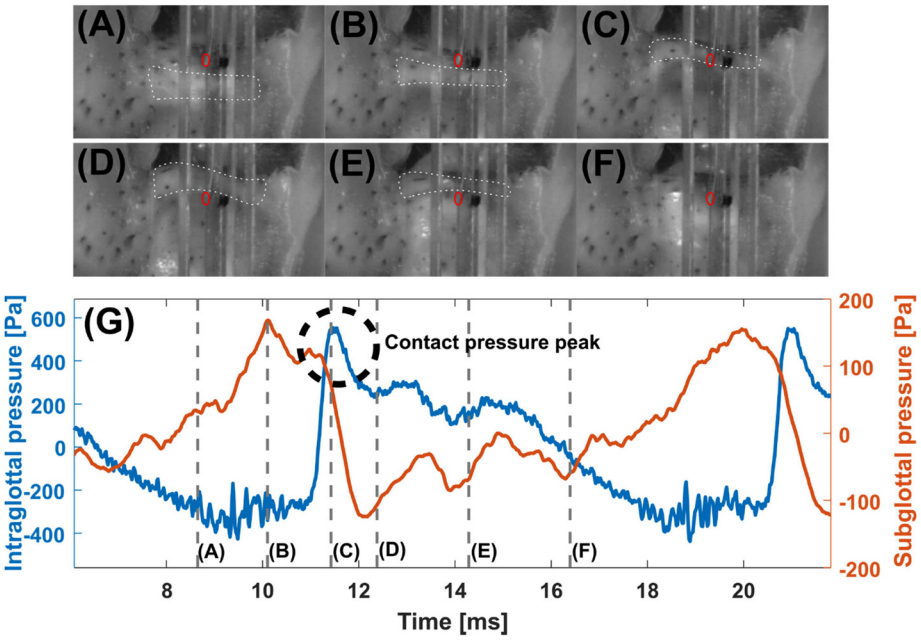

FIG. 6. High-speed video images [top panels (a)–(f)] of the medial surface motion at six consecutive instants within one oscillating cycle and the corresponding intraglottal and subglottal pressure waveforms (g). On each high-speed video image, a red circle is used to indicate the location of the sensing element, and the mucosal wave front is highlighted in white dotted lines. The time instants corresponding to each frame are indicated on panel (g) by vertical dashed gray lines. In addition, the contact pressure peak is indicated by a black dashed circle. Multimedia available online.

location of the sensing element is highlighted by a red circle for clarity. Due to the use of a prism in this setup, these images were captured at an angle of about 45° with respect to the plane of the acrylic plate.

In this recording, the frame shown in Fig. 6(b) (Multimedia view) corresponds to the instant of maximum subglottal pressure, which is expected to approximately correlate with the moment of vocal fold contact. However, in this case, the sensing element was slightly higher than the lowest point of contact. Because of the wave-like motion of the vocal fold surface, the point of contact progressively moves upward after initial contact and reaches the sensing element only at the frame shown in Fig. 6(c) (Multimedia view), corresponding to the highest peak in the intraglottal pressure as shown in Fig. 6(g) (Multimedia view). After this moment, the point of contact keeps moving upward until vocal fold decontacting. The pressure fluctuations measured after this point are due to aerodynamic flow pressure.

C. Variations in the contact pressure distribution for different laryngeal configurations

Figure 7 displays the pressure distribution for two different laryngeal configurations of the same larynx, one where the vocal folds are thin and elongated [Fig. 7(a)] and the other where the vocal folds are

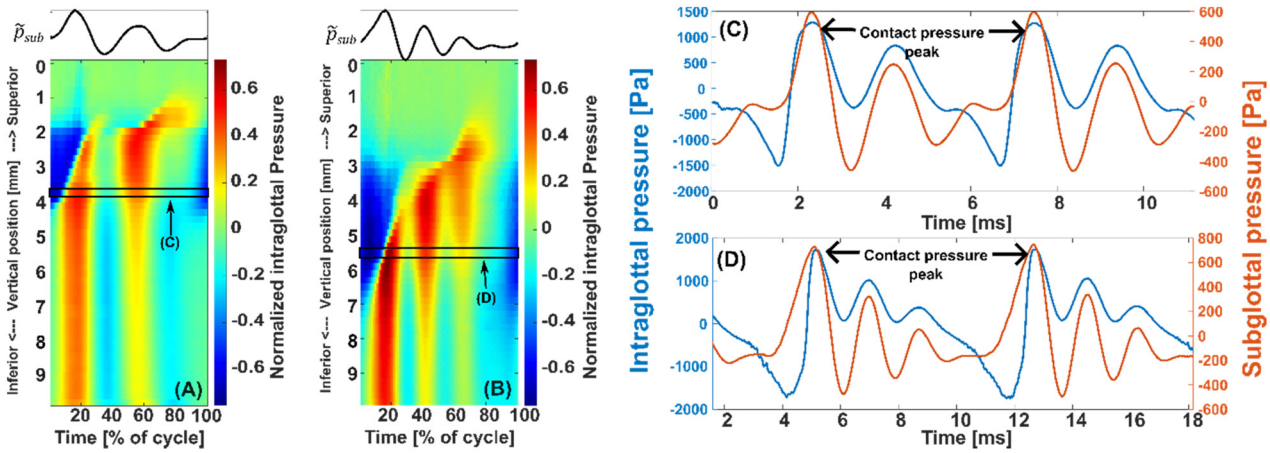

FIG. 7. Comparison of the intraglottal pressure distribution and waveform for two different laryngeal configurations. Panels (a) and (b) show the spatiotemporal map of the intraglottal pressure for the "thin" and "thick" conditions, respectively. Panels (c) and (d) show the corresponding time-varying intraglottal and subglottal pressure waveforms at the vertical locations indicated by the black rectangles in (a) and (b), respectively. In panels (c) and (d), the contact pressure peaks are indicated by black arrows. The fundamental frequency of oscillation was approximately 196 Hz for the "thin" condition and about 128 Hz for the "thick" condition. The mean subglottal pressure was 2.4 and 2.3 kPa for the "thin" and "thick" conditions, respectively.

lax, short and thick [Fig. 7(b)]. The data were from the full-larynx experiments. In the "thin" condition, 100 g weights were attached to the adduction sutures and 50 g weights were attached to the elongation sutures. The fundamental frequency was about 196 Hz on average. The "thick" condition is the one presented earlier in Subsection A, where weights of 50 g were attached to the adduction sutures, no weight was attached to the elongation sutures, and the thyroid cartilage was slightly pushed posteriorly. In this case, the fundamental frequency was about 128 Hz on average. While the vocal fold thickness is not a parameter that could be easily controlled nor measured here, the pressure distributions exhibit a visible difference regarding the vertical span of vocal fold contact: in the "thin" configuration [Fig. 7(a)], the contact area seems to span only about 2 mm, whereas in the "thick" configuration [Fig. 7(b)], the contact area spans about 3 mm.

Additionally, the right side of Fig. 7 shows the intraglottal and subglottal pressure waveforms around the vertical location of maximum contact pressure, for the two configurations. The intraglottal pressure waveform shape is not so different overall, but the contact pressure peak is broader in the "thin" configuration than in the "thick" configuration. The most significant difference here is the value of the maximum contact pressure: it reaches about 1250 Pa in the "thin" configuration and about 1750 Pa in the "thick" condition, while the mean subglottal pressure value was 2.4 and 2.3 kPa for the "thin" and "thick" conditions, respectively. In other words, for about the same mean subglottal pressure value, the peak vocal fold contact pressure value in the "thick" condition was about 40% higher than that in the "thin" condition. This effect of vertical thickness is consistent with findings from recent numerical simulations.[13,21–23]

IV. DISCUSSION

This study investigates the spatiotemporal distribution of intraglottal pressure and vocal fold contact pressure across the medial surface of the vocal folds, using excised larynges and a fine resolution grid. The resulting pressure maps provide an overview picture of the intraglottal and contact pressure distribution along both the vertical and anterior–posterior directions.

The specific goal of this study was to provide a basis for the investigation of contact pressure and its variations across different laryngeal configurations. While the contact pressure component of intraglottal pressure has been easily identified in previous studies as a sharp peak occurring before a longer, more rounded peak corresponding to aerodynamic flow pressure[2,5,7,11], in our study the presence of ripples in the intraglottal pressure waveform [as in Figs. 4(b)–4(d), 7(c), and 7(d)] made the identification of contact pressure more difficult. Through simple numerical simulations using Bernoulli's equation and a simplified vocal fold geometry, a more robust criterion was obtained to identify the contact pressure peak in the intraglottal pressure waveform: the contact pressure component should consist of a rapid increase occurring immediately after a negative pressure. In Fig. 4(d), this corresponds to the peak around 2 ms.

Using this criterion to locate the zone of vocal fold contact, the pressure distribution maps are particularly useful to determine the vertical span of vocal fold contact, such as in the ones presented in Figs. 3, 4(a), 7(a), and 7(b): a band can be identified where the pressure goes to very low negative values (blue color on the figures) right before having a rapid increase, indicating vocal fold contact. This band is expected to indicate the vertical span of vocal fold contact, which by extension can provide an estimate of vocal fold vertical thickness. This parameter is not easily controlled nor measured *ex vivo* or *in vivo*, but it has been shown to have a substantial impact on the value of contact pressure and other voice outcome measures.[13,21–23] In the current study, a notable difference in the peak contact pressure value was observed between the "thin" [Figs. 7(a) and 7(c)] and the "thick" [Figs. 7(b) and 7(d)] conditions, which corroborates the findings from those previous numerical studies. More excised larynx experiments need to be performed to confirm these findings.

The pressure distribution maps also allow estimation of mucosal wave speed. Direct measurement of mucosal wave speed along the medial surface requires imaging of the medial surface, which is difficult in a full-larynx setting. In the pressure distribution maps, the transition between the negative intraglottal pressure and the contact pressure that immediately follows allows an indirect way to observe the mucosal wave propagation along the medial surface. Mucosal wave speed can be estimated from the slope of this transition region [e.g., Fig. 4(a)]. For the two conditions shown in Fig. 7, the mucosal wave speed value is estimated to be 3 m/s for the "thin" condition [Figs. 7(a) and 7(c)] and 1.8 m/s for the "thick" condition [Figs. 7(b) and 7(d)]. This is consistent with the values reported in previous studies[24,25]. The ratio of the two mucosal wave speeds (about 1.67) and the ratio of the fundamental frequency values (about 1.53) are very similar, suggesting that the method can provide reasonable estimates of the mucosal wave speed.

Interestingly, we did not observe substantial changes in the peak contact pressure value across different positions along the anterior–posterior dimension, which contrasts with the findings from Jiang and Titze[2] who found a difference in the peak contact pressure value as high as 40% between the middle and anterior or posterior parts of the glottis. One possible cause is that our anterior–posterior span (4 mm) was too small to see any substantial difference in the peak contact pressure values. Another potential cause could be the fact that the contact pressure measurements in our study were done with a full-larynx setup, where the probe was disrupting the vocal fold vibration. Because of the probe's presence, the variations in the amplitude of vibration—and by extension the variations in the contact pressure value—along the anterior–posterior axis may be smaller than they would be without the probe. Since we were able to measure the pressure only at one anterior–posterior location during the hemilarynx experiments, we could not confirm this hypothesis.

Only the results from one full larynx and one hemilarynx are reported here, as the results obtained from all larynges were mostly consistent: the variations of the intraglottal pressure waveform and amplitude were small along the anterior–posterior dimension but large along the vertical dimension, and the spatiotemporal patterns were very similar to Fig. 3. Fine details vary across different larynges depending on the degree of contact and other factors, and our future goal is to isolate and investigate the effects of those factors on contact pressure.

This study has three main limitations. The first limitation is, as previously mentioned, that the probe disrupted vocal fold vibration during the full-larynx experiments, even though its outer diameter was only 1.24 mm. This means that the vocal fold could not vibrate to their full extent, and therefore, the contact pressure measured with this setup can only be considered an approximation of the contact pressure between the two opposing vocal fold medial surfaces, suggesting the contact pressure values presented here should be interpreted with caution. Additionally, because of the difficulty of placing

the probe exactly at the glottal centerline, its impact may have been slightly different on each vocal fold, as mentioned in the Methods section. The placement of the sensor in the medial–lateral dimension may have a large impact on vocal fold vibrations and, therefore, on contact patterns. Nevertheless, we believe that the results from the full-larynx experiments are useful and relevant for comparison with the measurement of contact pressure in living human subjects, where contact pressure cannot be measured without disrupting vocal fold vibration. The second limitation of our study is the methodology used to synchronize recordings at different locations cycle-wise and obtain the pressure distribution maps. This synchronization method requires the vocal fold vibration pattern to remain stationary throughout the duration of experiments. Therefore, this method cannot be applied to irregular phonation that could occur for example in subjects experiencing a decreased voice quality due to phonotrauma. The last limitation is the inability of the probe microphone to measure the mean component of the intraglottal pressure. It has been shown, through simulations[18] and experiments[16], that the mean component of the pressure greatly varies along the glottal channel, from a very small value in the supraglottal space to the value of the mean subglottal pressure in the subglottal space. The mean component of the pressure could be used, for example, to identify the transition from intraglottal to subglottal space more easily, as done in the experimental study by Mehta *et al.*[5]

V. CONCLUSIONS

In this study, a novel method is presented to measure and visualize the spatiotemporal distribution of intraglottal pressure and vocal fold contact pressure over the vocal fold medial surface along both vertical and anterior–posterior dimensions. Results show that the amplitude and waveform patterns of the intraglottal pressure only exhibit small variations along the anterior–posterior dimension, whereas both the amplitude and waveform shape of the intraglottal pressure greatly vary along the vertical dimension. Criteria based on theory and experiment are developed to identify the vocal fold contact pressure peak in the intraglottal pressure waveform, which allows estimation of the vertical span of vocal fold contact and mucosal wave speed. Preliminary results show that increasing vocal fold vertical thickness significantly increases the peak vocal fold contact pressure value.

SUPPLEMENTARY MATERIAL

See the supplementary material for the File SP01: ZIP archive containing two STEP files of the anterior and posterior parts of the sliding acrylic piece described in Fig. 2.

ACKNOWLEDGMENTS

We would like to thank Yazeed Alhiyari for his help with 3D-printing parts of our experimental setup. This work was supported by the research Grant No. R01 DC020240 from the National Institute on Deafness and Other Communication Disorders, the National Institutes of Health.

AUTHOR DECLARATIONS

Conflict of Interest

The authors have no conflicts to disclose.

Ethics Approval

This study used excised larynges from animals and human individuals that were not sacrificed for the purpose of this study, and therefore, the experiments did not require ethical approval.

Author Contributions

Sarah Lehoux: Data curation (equal); Formal analysis (equal); Investigation (equal); Methodology (equal); Visualization (equal); Writing – original draft (equal); Writing – review & editing (equal). **Zhaoyan Zhang:** Conceptualization (lead); Funding acquisition (lead); Investigation (supporting); Methodology (equal); Project administration (lead); Resources (lead); Supervision (lead); Validation (lead); Writing – review & editing (equal).

DATA AVAILABILITY

The data that support the findings of this study are available from the corresponding author upon reasonable request.

APPENDIX: DERIVATION OF EQUATION (1)

Assuming a one-dimensional, incompressible, steady, inviscid flow, and a negligible gravitational change along the glottal channel, Bernoulli's equation can be expressed for two points along the glottal channel as

$$P_1 - P_2 = \frac{\rho}{2}\left(v_2^2 - v_1^2\right), \tag{A1}$$

where P_1 and P_2 are the pressures at the two points along the glottal channel, ρ is the density of the fluid, and v_1 and v_2 are the particle velocities at those two points. If the points are chosen as the flow separation point (considered here as the upper margin of the vocal folds for simplicity) and a point upstream of this point, as depicted in Fig. 8, and if the velocities are expressed as the volume flow rate u divided by the cross-sectional area A, Eq. (A1) can be written as

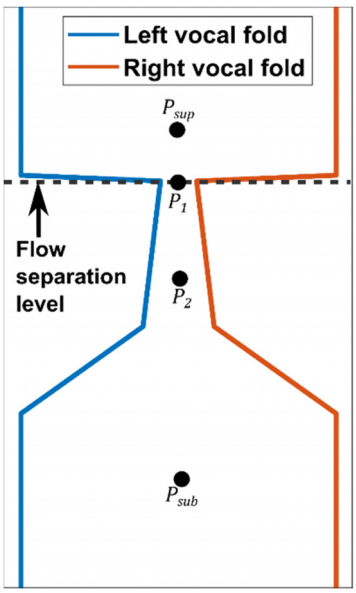

FIG. 8. Drawing of a simple glottal channel geometry.

$$P_1 - P_2 = \frac{\rho}{2}u^2\left(\frac{1}{A_2^2} - \frac{1}{A_{sep}^2}\right), \tag{A2}$$

where A_{sep} is the cross-sectional area at the flow separation point, and A_2 is the cross-sectional area at the point upstream. If the point upstream is chosen to be in the subglottal space (P_{sub} in Fig. 8), then Eq. (A2) becomes

$$P_1 - P_{sub} = \frac{\rho}{2}u^2\left(\frac{1}{A_{sub}^2} - \frac{1}{A_{sep}^2}\right), \tag{A3}$$

where A_{sub} is the cross-sectional area in the subglottal space. Since the cross-sectional area of the subglottal space is much larger than the cross-sectional area in the glottis, the term $\frac{1}{A_{sub}^2}$ can be omitted in Eq. (A3). From Eq. (A3), the term $\frac{\rho}{2}u^2$ can be expressed as

$$\frac{\rho}{2}u^2 = A_{sep}^2(P_{sub} - P_1). \tag{A4}$$

Since P_1 is at the level of flow separation, it can be assumed to be equal to the pressure in the supraglottal space P_{sup}. Replacing P_1 by P_{sup} and substituting $\frac{\rho}{2}u^2$ in Eq. (A2), the value of P_2 can be expressed as

$$P_2 = P_{sup} + (P_{sub} - P_{sup})\left(1 - \frac{A_{sep}^2}{A_2^2}\right). \tag{A5}$$

Equation (1) is then obtained by replacing P_2 by the pressure P of any point within the glottal channel, upstream of the flow separation point, with the corresponding cross-sectional area A.

REFERENCES

[1]I. R. Titze, "Mechanical stress in phonation," J. Voice **8**(2), 99–105 (1994).
[2]J. J. Jiang and I. R. Titze, "Measurement of vocal fold intraglottal pressure and impact stress," J. Voice **8**(2), 132–144 (1994).
[3]K. Verdolini, D. G. Druker, P. M. Palmer, and H. Samawi, "Laryngeal adduction in resonant voice," J. Voice **12**(3), 315–327 (1998).
[4]K. Verdolini-Marston, M. Katherine Burke, A. Lessac, L. Glaze, and E. Caldwell, "Preliminary study of two methods of treatment for laryngeal nodules," J. Voice **9**(1), 74–85 (1995).
[5]D. D. Mehta, J. B. Kobler, S. M. Zeitels, M. Zañartu, B. D. Erath, M. Motie-Shirazi, S. D. Peterson, R. H. Petrillo, and R. E. Hillman, "Toward development of a vocal fold contact pressure probe: Bench-top validation of a dual-sensor probe using excised human larynx models," Appl. Sci. **9**(20), 4360 (2019).
[6]F. Alipour and R. C. Scherer, "Dynamic glottal pressures in an excised hemilarynx model," J. Voice **14**(4), 443–454 (2000).
[7]L.-J. Chen and L. Mongeau, "Verification of two minimally invasive methods for the estimation of the contact pressure in human vocal folds during phonation," J. Acoust. Soc. Am. **130**(3), 1618–1627 (2011).
[8]M. E. Díaz-Cádiz, S. D. Peterson, G. E. Galindo, V. M. Espinoza, M. Motie-Shirazi, B. D. Erath, and M. Zañartu, "Estimating vocal fold contact pressure from raw laryngeal high-speed videoendoscopy using a hertz contact model," Appl. Sci. **9**(11), 2384 (2019).
[9]M. Motie-Shirazi, M. Zañartu, S. D. Peterson, D. D. Mehta, J. B. Kobler, R. E. Hillman, and B. D. Erath, "Toward development of a vocal fold contact pressure probe: Sensor characterization and validation using synthetic vocal fold models," Appl. Sci. **9**(15), 3002 (2019).
[10]M. M. Hess, K. Verdolini, W. Bierhals, U. Mansmann, and M. Gross, "Endolaryngeal contact pressures," J. Voice **12**(1), 50–67 (1998).
[11]D. D. Mehta, J. B. Kobler, S. M. Zeitels, M. Zañartu, E. J. Ibarra, G. A. Alzamendi, R. Manriquez, B. D. Erath, S. D. Peterson, R. H. Petrillo, and R. E. Hillman, "Direct measurement and modeling of intraglottal, subglottal, and vocal fold collision pressures during phonation in an individual with a hemilaryngectomy," Appl. Sci. **11**(16), 7256 (2021).
[12]Z. Zhang, "Interaction between epilaryngeal and laryngeal adjustments in regulating vocal fold contact pressure," JASA Express Lett. **1**(2), 025201 (2021).
[13]Z. Zhang, "Laryngeal strategies to minimize vocal fold contact pressure and their effect on voice production," J. Acoust. Soc. Am. **148**(2), 1039–1050 (2020).
[14]Z. Zhang, "Vocal tract adjustments to minimize vocal fold contact pressure during phonation," J. Acoust. Soc. Am. **150**(3), 1609–1619 (2021).
[15]C. T. Herbst, V. Hampala, M. Garcia, R. Hofer, and J. G. Švec, "Hemi-laryngeal setup for studying vocal fold vibration in three dimensions," J. Vis. Exp. **129**, e55303 (2017).
[16]R. C. Scherer, S. Torkaman, B. R. Kucinschi, and A. A. Afjeh, "Intraglottal pressures in a three-dimensional model with a non-rectangular glottal shape," J. Acoust. Soc. Am. **128**(2), 828–838 (2010).
[17]Z. Zhang, "Mechanics of human voice production and control," J. Acoust. Soc. Am. **140**(4), 2614–2635 (2016).
[18]C. Guo and R. C. Scherer, "Finite element simulation of glottal flow and pressure," J. Acoust. Soc. Am. **94**(2), 688–700 (1993).
[19]J. G. Švec, H. K. Schutte, J. C. Chen, and I. R. Titze, "Integrative insights into the myoelastic-aerodynamic theory and acoustics of phonation. Scientific tribute to Donald G. Miller," J. Voice **37**(3), 305–313 (2023).
[20]D. G. Miller and H. K. Schutte, "Characteristic patterns of sub- and supraglottal pressure variations within the glottal cycle," in *Transcripts of the XIIIth Symposium: Care for the Professional Voice* (The Voice Foundation, 1985), pp. 70–75.
[21]Z. Zhang, "Interaction effects in laryngeal and respiratory control of the voice source and vocal fold contact pressure," J. Acoust. Soc. Am. **156**(6), 4326–4335 (2024).
[22]Z. Zhang, "Vocal fold vertical thickness in human voice production and control: A review," J. Voice **22**, S0892-1997(23)00078-4 (2023).
[23]I. McCollum, A. Throop, D. Badr, and R. Zakerzadeh, "Gender in human phonation: Fluid–structure interaction and vocal fold morphology," Phys. Fluids **35**(4), 041907 (2023).
[24]I. R. Titze, J. J. Jiang, and T.-Y. Hsiao, "Measurement of mucosal wave propagation and vertical phase difference in vocal fold vibration," Ann. Otol. Rhinol. Laryngol. **102**(1), 58–63 (1993).
[25]A. Boessenecker, D. A. Berry, J. Lohscheller, U. Eysholdt, and M. Doellinger, "Mucosal wave properties of a human vocal fold," Acta Acust. Acust. **93**(5), 815–823 (2007).